Axion-Like Particles, Two-Higgs-Doublet Models, Leptoquarks, and the Electron and Muon $g - 2$

Wai-Yee Keung,[1] Danny Marfatia,[2] and Po-Yan Tseng[3]

[1]*Department of Physics, University of Illinois at Chicago, Illinois 60607 USA*

[2]*Department of Physics & Astronomy, University of Hawaii at Manoa, Honolulu, HI 96822, USA*

[3]*Department of Physics and IPAP, Yonsei University, Seoul 03722, Republic of Korea*

Abstract

Data from the Muon $g - 2$ experiment and measurements of the fine structure constant suggest that the anomalous magnetic moments of the muon and electron are at odds with standard model expectations. We survey the ability of axion-like particles, two-Higgs-doublet models and leptoquarks to explain the discrepancies. We find that accounting for other constraints, all scenarios except the Type-I, Type-II and Type-Y two-Higgs-doublet models fit the data well.

1. INTRODUCTION

The high-intensity and high-precision frontiers are ideal for the search for new physics that couples very feebly with the standard model (SM) sector. A long-standing and perhaps best known example that indicates such physics is the 3.7σ anomaly in the anomalous magnetic moment of the muon $a_\mu = (g - 2)_\mu/2$:

$$\Delta a_\mu^{\text{BNL}} = a_\mu^{\text{BNL}} - a_\mu^{\text{SM}} = (279 \pm 76) \times 10^{-11}, \quad (1)$$

where $a_\mu^{\text{BNL}} = (116592089 \pm 63) \times 10^{-11}$ [1, 2] and the SM expectation is $a_\mu^{\text{SM}} = (116591810 \pm 43) \times 10^{-11}$ [3]. A new lattice QCD calculation of the hadronic vacuum polarization suggests that the BNL measurement is compatible with the SM and that no new physics need to be incorporated [4]. Until this result is confirmed, we subscribe to the SM value of ref. [3]. Recently, the Muon $g - 2$ experiment at Fermilab reported the value, $a_\mu^{\text{FNAL}} = (116592040 \pm 54) \times 10^{-11}$ [5], i.e.,

$$\Delta a_\mu^{\text{FNAL}} = a_\mu^{\text{FNAL}} - a_\mu^{\text{SM}} = (230 \pm 69) \times 10^{-11}, \quad (2)$$

which is a 3.3σ discrepancy. The combined significance of the anomaly from the Fermilab and BNL measurements is 4.25σ with [5]

$$\Delta a_\mu = a_\mu^{\text{exp}} - a_\mu^{\text{SM}} = (251 \pm 59) \times 10^{-11}. \quad (3)$$

Interestingly, new precise measurements of the fine-structure constant α imply a discrepancy in the anomalous magnetic moment of the electron as well. A measurement of α at Laboratoire Kastler Brossel (LKB) with ^{87}Rb atoms [6] improves the accuracy by a factor of 2.5 compared to the previous best measurement with ^{137}Cs atoms at Berkeley [7]. The LKB measurement deviates by 5.4σ from the Berkeley result. With these two measurements of α, the SM predictions for the electron anomalous magnetic moments, a_e^{LKB} and a_e^{B} [8, 9], differ from the experimental measurement a_e^{exp} [10] at 1.6σ and 2.4σ, respectively:

$$\Delta a_e^{\text{LKB}} = a_e^{\text{exp}} - a_e^{\text{LKB}} = (4.8 \pm 3.0) \times 10^{-13},$$
$$\Delta a_e^{\text{B}} = a_e^{\text{exp}} - a_e^{\text{B}} = (-8.8 \pm 3.6) \times 10^{-13}. \quad (4)$$

Note the opposite signs of Δa_e^{LKB} and Δa_e^{B}.

In this work, we study how well pseudoscalar axion-like particles (ALPs), two-Higgs-doublet models (2HDMs), and leptoquarks (LQs) can provide a common explanation of the anomalies in Δa_μ and $\Delta a_e^{\text{LKB,B}}$.

2. AXION-LIKE PARTICLES

An ALP, in general, can couple to the photon and leptons via the effective interactions [16],

$$\mathcal{L} \supset \frac{1}{4} g_{a\gamma\gamma} a F_{\mu\nu} \tilde{F}^{\mu\nu} + i y_{a\ell} a \bar{\ell} \gamma_5 \ell, \quad (5)$$

where $g_{a\gamma\gamma}$ is a dimensionful coupling, and $F_{\mu\nu}$ and $\tilde{F}^{\mu\nu}$ are the electromagnetic tensor and its dual, respectively. We can take $g_{a\gamma\gamma}$ to be positive by absorbing a phase into the definition of the field a. Then the sign of $y_{a\ell}$ becomes physical. If Λ is the ultraviolet cut-off of the effective theory, $g_{a\gamma\gamma} = 2\sqrt{2}\alpha c_{a\gamma\gamma}/\Lambda$ with dimensionless coupling $c_{a\gamma\gamma}$. The first term in Eq. (5) induces the two loop light-by-light (LbL) diagram which is analogous to the SM hadronic contribution from π^0 exchange [11, 12, 13]. Both terms in Eq. (5) contribute to $g - 2$ via Barr-Zee (BZ) diagrams [14]. By only keeping the leading log, these contributions to a_ℓ give

$$a_{\ell,a} = a_{\ell,a}^{1-\text{loop}} + a_{\ell,a}^{\text{BZ}} + a_{\ell,a}^{\text{LbL}}, \quad \text{where}$$
$$a_{\ell,a}^{1-\text{loop}} \simeq \frac{y_{a\ell}^2}{8\pi^2} \left(\frac{m_\ell}{m_a}\right)^2 f_A(m_\ell^2/m_a^2) \text{ [15]},$$
$$a_{\ell,a}^{\text{BZ}} \simeq \frac{m_\ell}{4\pi^2} g_{a\gamma\gamma} y_{a\ell} \ln \frac{\Lambda}{m_a} \text{ [16]},$$
$$a_{\ell,a}^{\text{LbL}} \simeq 3\frac{\alpha}{\pi} \left(\frac{m_\ell g_{a\gamma\gamma}}{4\pi}\right)^2 \left(\ln \frac{\Lambda}{m_a}\right)^2 \text{ [16]}. \quad (6)$$

Here, m_a is the ALP mass and the one-loop function for a pseudoscalar is [15]

$$f_A(r) = \int_0^1 dx \frac{-x^3}{1 - x + rx^2}. \quad (7)$$

ALP masses between $0.1\,\text{GeV}$ to $10\,\text{GeV}$ are allowed for non-negligible $g_{a\gamma\gamma}$ [17]. In particular, $m_a \leq 0.1\,\text{GeV}$ is restricted by beam dump experiments, and LEP data on the decay $Z \to 3\gamma$ constrains $m_a \geq 10\,\text{GeV}$ via the process $e^+ e^- \to$
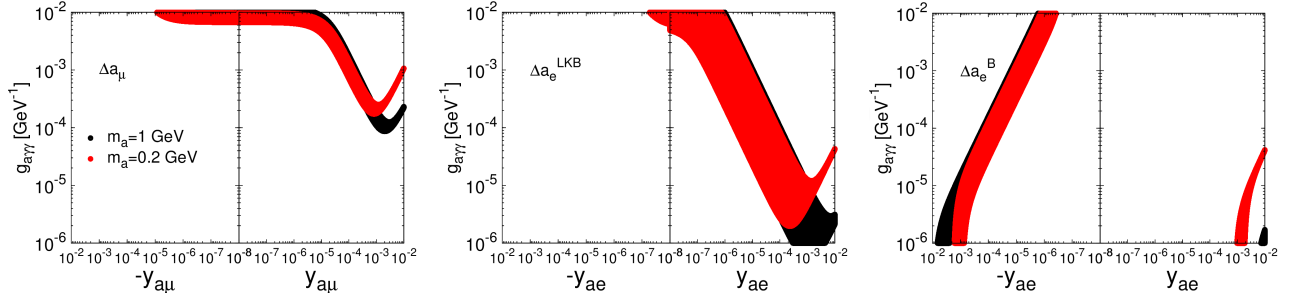
FIGURE 1: ALP-1: The 1σ regions preferred by Δa_μ, Δa_e^{LKB}, and Δa_e^{B} for $m_a = 1\,\text{GeV}$ (black) and $m_a = 0.2\,\text{GeV}$ (red).
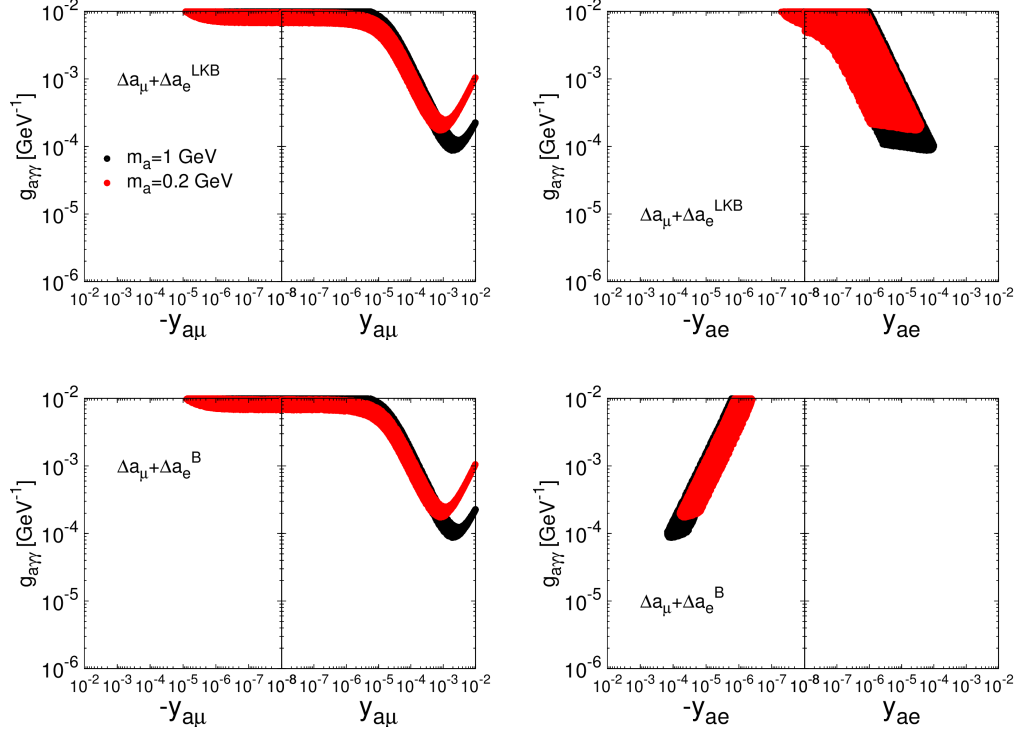
FIGURE 2: ALP-1: The 1σ allowed regions from a combined fit to Δa_μ and Δa_e^{LKB} (upper panels) and Δa_μ and Δa_e^{B} (lower panels), for $m_a = 1\,\text{GeV}$ (black) and $m_a = 0.2\,\text{GeV}$ (red).

	y_u^A	y_d^A	y_ℓ^A	y_u^H	y_d^H	y_ℓ^H	y_u^h	y_d^h	y_ℓ^h
Type-I	$\cot\beta$	$-\cot\beta$	$-\cot\beta$	$\frac{\sin\alpha}{\sin\beta}$	$\frac{\sin\alpha}{\sin\beta}$	$\frac{\sin\alpha}{\sin\beta}$	$\frac{\cos\alpha}{\sin\beta}$	$\frac{\cos\alpha}{\sin\beta}$	$\frac{\cos\alpha}{\sin\beta}$
Type-II	$\cot\beta$	$\tan\beta$	$\tan\beta$	$\frac{\sin\alpha}{\sin\beta}$	$\frac{\cos\alpha}{\cos\beta}$	$\frac{\cos\alpha}{\cos\beta}$	$\frac{\cos\alpha}{\sin\beta}$	$-\frac{\sin\alpha}{\cos\beta}$	$-\frac{\sin\alpha}{\cos\beta}$
Type-X	$\cot\beta$	$-\cot\beta$	$\tan\beta$	$\frac{\sin\alpha}{\sin\beta}$	$\frac{\sin\alpha}{\sin\beta}$	$\frac{\cos\alpha}{\cos\beta}$	$\frac{\cos\alpha}{\sin\beta}$	$\frac{\cos\alpha}{\sin\beta}$	$-\frac{\sin\alpha}{\cos\beta}$
Type-Y	$\cot\beta$	$\tan\beta$	$-\cot\beta$	$\frac{\sin\alpha}{\sin\beta}$	$\frac{\cos\alpha}{\cos\beta}$	$\frac{\sin\alpha}{\sin\beta}$	$\frac{\cos\alpha}{\sin\beta}$	$-\frac{\sin\alpha}{\cos\beta}$	$\frac{\cos\alpha}{\sin\beta}$

TABLE 1: The normalized Yukawa couplings for the two-Higgs-doublet models [19].

	Type-I		Type-II		Type-X		Type-Y	
	LKB	B	LKB	B	LKB	B	LKB	B
m_A/GeV	98.5	98.5	3.44	99.2	6.52	71.5	99.8	99.8
$\tan\beta$	99.4	99.4	40.9	88.1	68.9	99.3	94.3	94.3
a_μ	-1.5×10^{-11}	-1.5×10^{-11}	2.5×10^{-9}	2.4×10^{-9}	2.5×10^{-9}	2.5×10^{-9}	-1.6×10^{-11}	-1.6×10^{-11}
a_e	-3.6×10^{-16}	-3.6×10^{-16}	4.8×10^{-13}	5.8×10^{-14}	4.9×10^{-13}	6.5×10^{-14}	-3.7×10^{-16}	-3.7×10^{-16}
χ^2_{LKB}	20.9	—	0	—	0	—	20.9	—
χ^2_{B}	—	24.3	—	6.81	—	6.90	—	24.3

TABLE 2: Best-fit points, their contributions to the anomalous magnetic moments, and minimum χ^2 values for the 2HDMs.
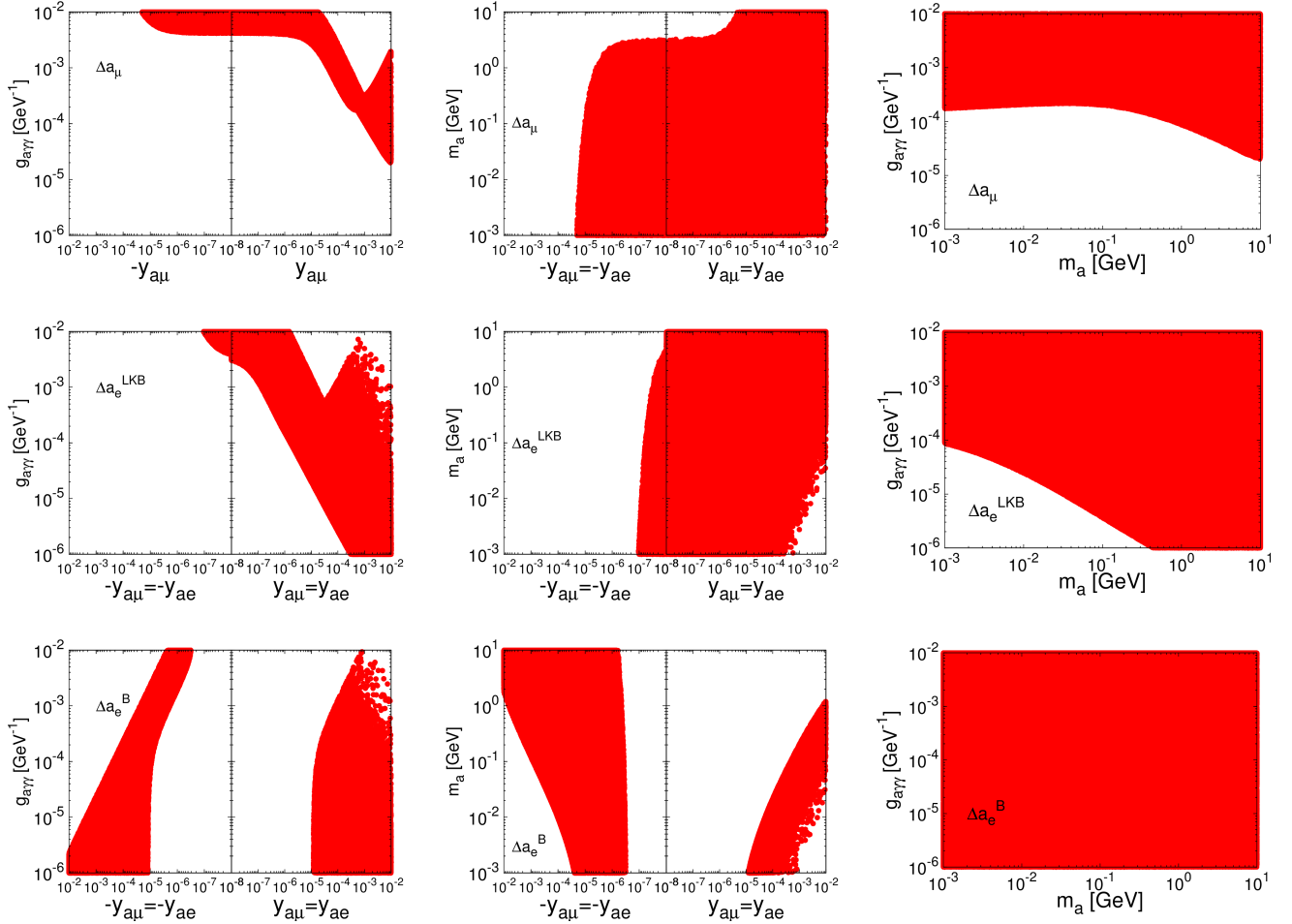
FIGURE 3: ALP-2: The 1σ regions preferred by Δa_μ (upper panels), Δa_e^{LKB} (middle panels), and Δa_e^{B} (lower panels) for $y_{a\mu} = y_{ae}$.

	S_1-**LQ**				R_2-**LQ**			
	LKB	LKB	B	B	LKB	LKB	B	B
$m_{S_1(R_2)}/$TeV	2	10	2	10	2	10	2	10
$y_{ec}^L y_{ec}^R$	1.1×10^{-2}	0.20	-1.9×10^{-2}	-0.37	-8.3×10^{-3}	-0.16	1.5×10^{-2}	0.30
$y_{\mu t}^L y_{\mu t}^R$	1.6×10^{-2}	0.12	1.5×10^{-2}	0.12	-4.7×10^{-3}	-6.9×10^{-2}	-4.7×10^{-3}	-6.8×10^{-2}

TABLE 3: Best-fit points for the scalar and doublet leptoquarks. The minimum χ^2 value in all cases is 0.

$\gamma^* \rightarrow a\gamma \rightarrow 3\gamma$ [18]. Also, $Z \rightarrow 2\gamma$ data at LEP provide a constraint if photons from $a \rightarrow 2\gamma$ are collimated as a single photon. An upper bound $g_{a\gamma\gamma} \simeq \mathcal{O}(10^{-2})\,\text{GeV}^{-1}$ is obtained for $1\,\text{MeV} \leq m_a \leq 10\,\text{GeV}$ [17]. For this coupling, unitarity requires an upper bound, $\Lambda \simeq 1\,\text{TeV}$ [16].

To obtain parameter values preferred by the data, we separately fit Δa_μ, Δa_e^{LKB}, and Δa_e^{B}, and also fit the combinations, Δa_μ and Δa_e^{LKB}, and Δa_μ and Δa_e^{B}. We do not fit Δa_e^{LKB} and Δa_e^{B} simultaneously. We use the following χ^2 definitions:

$$\chi^2_{a_\mu} \equiv \frac{(a_{\mu,a} - \Delta a_\mu)^2}{(\sigma_{\Delta a_\mu})^2}, \quad \chi^2_{a_e^{\text{LKB}}} \equiv \frac{(a_{e,a} - \Delta a_e^{\text{LKB}})^2}{(\sigma_{\Delta a_e^{\text{LKB}}})^2},$$

$$\chi^2_{a_e^{\text{B}}} \equiv \frac{(a_{e,a} - \Delta a_e^{\text{B}})^2}{(\sigma_{\Delta a_e^{\text{B}}})^2}, \quad \chi^2_{\text{LKB}} \equiv \chi^2_{a_\mu} + \chi^2_{a_e^{\text{LKB}}}, \quad \chi^2_{\text{B}} \equiv \chi^2_{a_\mu} + \chi^2_{a_e^{\text{B}}}.$$

(8)

Similar definitions will apply for 2HDMs and leptoquarks.

Guided by the constraints mentioned above, we scan the parameter space in two scenarios which have the same number of free parameters:

- **ALP-1:** We fix $m_a = 0.2, 1\,\text{GeV}$, and vary $g_{a\gamma\gamma}$, $y_{a\mu}$, and y_{ae}. The results are shown in Figures 1 and 2.

- **ALP-2:** We vary m_a, $g_{a\gamma\gamma}$ and $y_{a\mu} = y_{ae}$. The results are shown in Figures 3 and 4.

The minimum χ^2 value in all cases is zero indicating that the deviations from the SM predictions can be exactly reproduced. Since the χ^2 distributions are very shallow around the minima, we do do not provide best-fit ALP points.

In the left panel of Figure 1, the plateau for small Yukawa couplings arises from the LbL contribution. For large negative $y_{a\mu}$, the BZ and 1-loop contributions interfere destructively with the LbL contribution which requires large $g_{a\gamma\gamma}$ values excluded by beam-dump experiments. For large positive $y_{a\mu}$ the
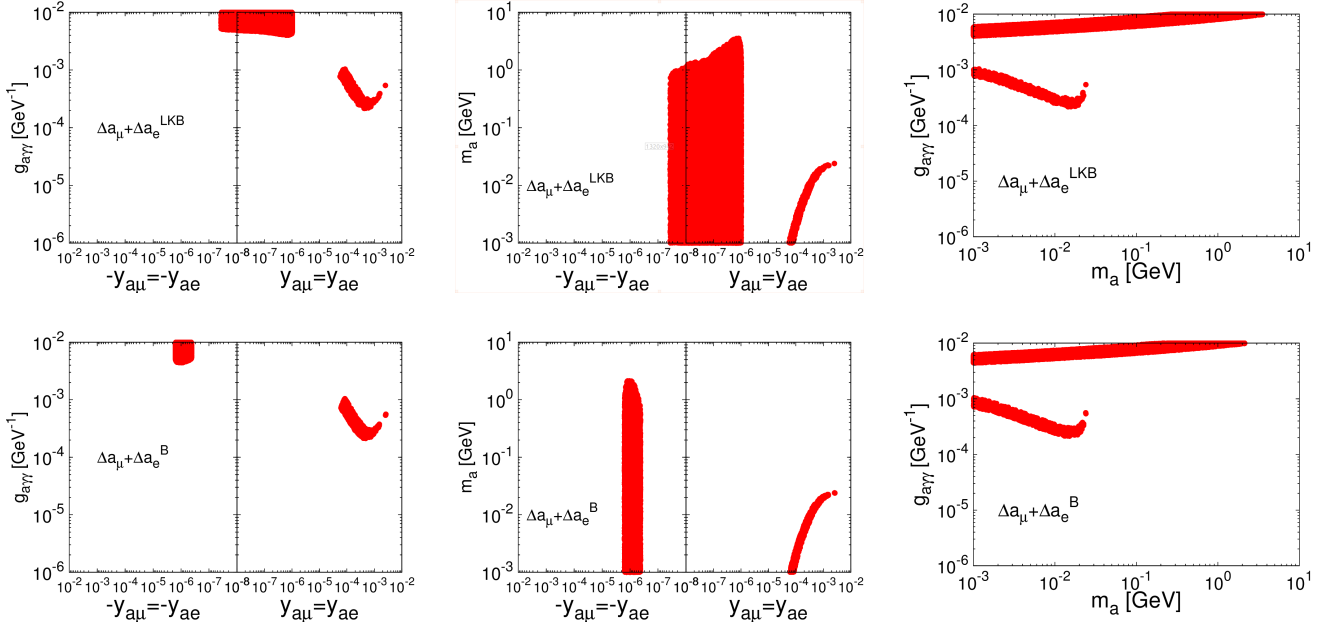
FIGURE 4: ALP-2: The 1σ allowed regions from a combined fit to Δa_μ and Δa_e^{LKB} (upper panels) and Δa_μ and Δa_e^{B} (lower panels), for $y_{a\mu} = y_{ae}$.
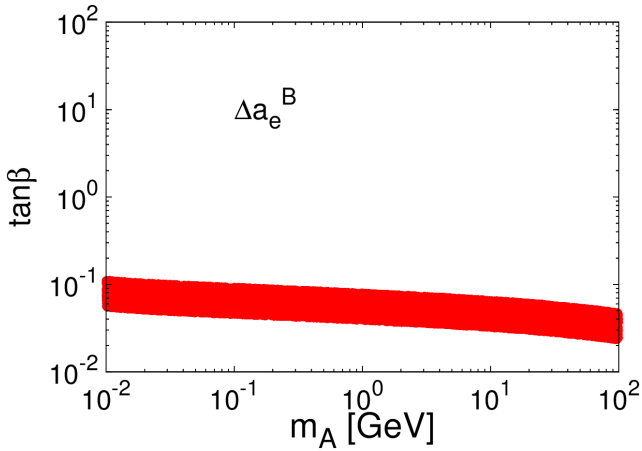
FIGURE 5: Type-I 2HDM: The 1σ region preferred by Δa_e^{B}. There is no solution for Δa_μ or Δa_e^{LKB} with $\chi^2 < 6.18$ (corresponding to 2σ for two parameters).

BZ and LbL contributions interfere constructively so that the size of $g_{a\gamma\gamma}$ is reduced to fit the data. However, as $y_{a\mu}$ increases, the 1-loop contribution interferes destructively with the BZ and LbL contributions, which causes $g_{a\gamma\gamma}$ to rise again. A similar reasoning explains the structure of the a_e^{LKB} allowed region. A plateau does not appear in the allowed region for Δa_e^{B} because it is negative.

3. TWO-HIGGS-DOUBLET MODELS

We now consider two-Higgs-doublet models. In addition to the light Higgs h, the scalar sector is comprised of a heavy Higgs

H, pseudoscalar A, and two charge Higgses $H^\pm$, which contribute to the electron and muon $g - 2$ through either 1-loop triangle diagrams or two-loop BZ diagrams. There are five relevant parameters, m_A, m_H, $m_{H^\pm}$, β, and α. The ratio of the vacuum expectation values of the two scalar doublets $\Phi_{1,2}$ defines $\tan\beta \equiv v_2/v_1$. The mixing between the CP-even neutral components $h_{1,2}$ of $\Phi_{1,2}$, and the mass eigenstates h, H is given by the angle α [19]:

$$h = h_1 \sin\alpha - h_2 \cos\alpha,$$
$$H = -h_1 \cos\alpha - h_2 \sin\alpha. \qquad (9)$$

To satisfy the stringent constraints on flavor changing neutral currents, the up-type quarks, down-type quarks and leptons must have Yukawa couplings to Φ_1 or Φ_2, but not both. This requirement leads to four types of 2HDMs: Type-I (all fermions couple to Φ_2), Type-II (only up-type quarks couple to Φ_2), Type-X (lepton-specific, in which only leptons couples to Φ_2), Type-Y (flipped, in which only down-type quarks couples to Φ_1) [19, 15]. The rare decay $b \to s\gamma$ requires $m_{H^\pm} \geq 300\,\text{GeV}$ for $\tan\beta \geq 2$ for Type-I and Type-X [19] ($m_{H^\pm} \geq 580\,\text{GeV}$ for Type-II and Type-Y [20]), which renders their contributions to $g - 2$ subdominant. Higgs precision measurements from ATLAS and CMS prefer h to be SM-like with $\cos(\beta - \alpha) \to 0$, and H decoupled. After fixing $m_h = 125.5\,\text{GeV}$, we are left with only two parameters m_A and $\tan\beta$ that affect $g - 2$. The Yukawa interactions in four types of 2HDMs are dictated by $\tan\beta$:

$$-\mathcal{L}_{\text{2HDM}}^{\text{Yukawa}} = \sum_{f=u,d,\ell} \frac{m_f}{v_{\text{EW}}} (y_f^h h \bar{f} f + y_f^H H \bar{f} f - i y_f^A \bar{f} \gamma_5 f)$$
$$+ \left[\sqrt{2} V_{ud} H^+ \bar{u} \left(\frac{m_u}{v_{\text{EW}}} y_u^A P_L + \frac{m_d}{v_{\text{EW}}} y_d^A P_R \right) d \quad (10)\right.$$
$$\left. + \frac{\sqrt{2} m_\ell}{v_{\text{EW}}} H^+ \bar{\nu} P_R \ell + h.c. \right],$$
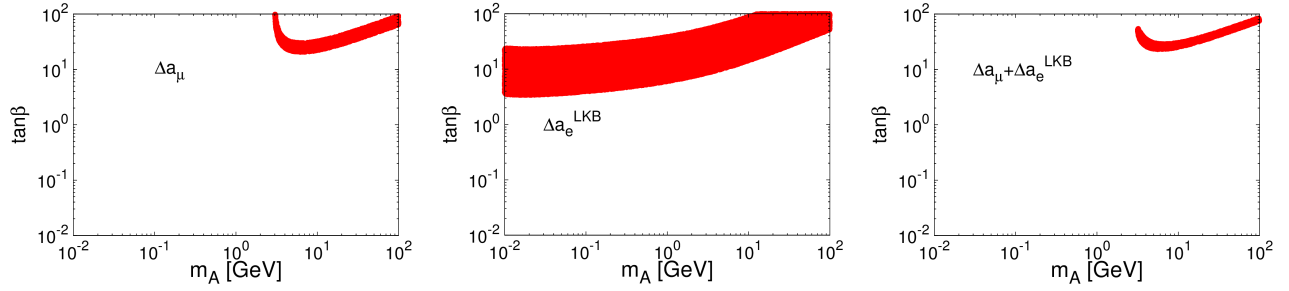
FIGURE 6: Type-II 2HDM: The 1σ regions preferred by Δa_μ, $\Delta a_e^{\mathrm{LKB}}$, and a combined fit of Δa_μ and $\Delta a_e^{\mathrm{LKB}}$. There is no solution for Δa_e^{B} with $\chi^2 < 6.18$.
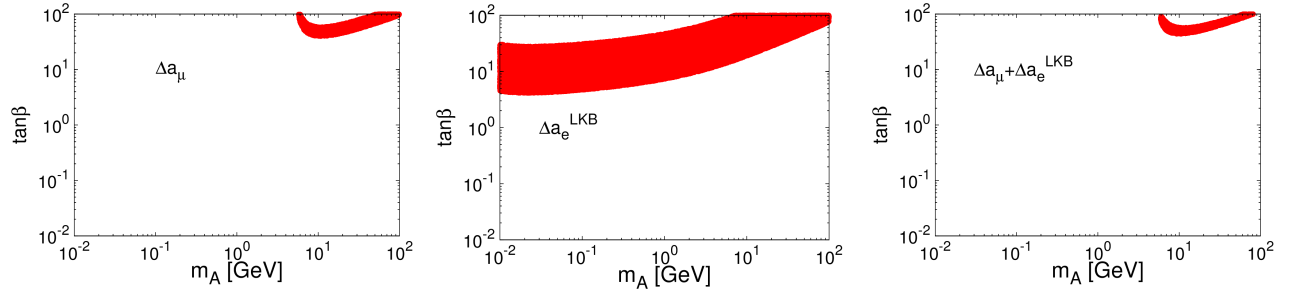
FIGURE 7: Type-X 2HDM: The 1σ regions preferred by Δa_μ, $\Delta a_e^{\mathrm{LKB}}$, and a combined fit of Δa_μ and $\Delta a_e^{\mathrm{LKB}}$. There is no solution for Δa_e^{B} with $\chi^2 < 6.18$.
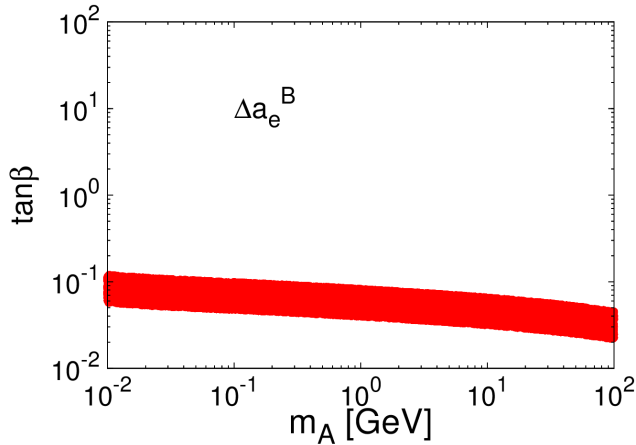
FIGURE 8: Type-Y 2HDM: The 1σ region preferred by Δa_e^{B}. There is no solution for Δa_μ or $\Delta a_e^{\mathrm{LKB}}$ with $\chi^2 < 6.18$.

with the normalized Yukawa couplings as listed in Table 1. The contribution to the anomalous magnetic moments is [15]

$$a_{\ell,\mathrm{2HDM}} = a_{\ell,\mathrm{2HDM}}^{1-\mathrm{loop}} + a_{\ell,\mathrm{2HDM}}^{\mathrm{BZ}}, \quad \text{where}$$

$$a_{\ell,\mathrm{2HDM}}^{1-\mathrm{loop}} = \frac{G_F m_\ell^2}{4\pi^2\sqrt{2}} \sum_{j=\{h,H,A,H^\pm\}} (y_\ell^j)^2 r_\ell^j f_j(r_\ell^j),$$

$$a_{\ell,\mathrm{2HDM}}^{\mathrm{BZ}} = \frac{G_F m_\ell^2}{4\pi^2\sqrt{2}} \frac{\alpha}{\pi} \sum_{i=\{h,H,A\};f=\{t,b,\tau\}} N_f^c Q_f^2 y_\ell^i y_f^i r_f^i g_i(r_f^i),$$

$$(11)$$

where $r_\ell^j \equiv m_\ell^2/m_j^2$, $r_f^i \equiv m_f^2/m_i^2$, and m_f, Q_f, N_f^c are the mass, electric charge and color factor for fermion f in the loop. The loop functions are

$$f_{h,H}(r) = \int_0^1 dx \frac{x^2(2-x)}{1-x+rx^2},$$

$$f_{H^\pm}(r) = \int_0^1 dx \frac{-x(1-x)}{1-r(1-x)},$$

$$g_{h,H}(r) = \int_0^1 dx \frac{2x(1-x)-1}{x(1-x)-r} \ln \frac{x(1-x)}{r},$$

$$g_A(r) = \int_0^1 dx \frac{1}{x(1-x)-r} \ln \frac{x(1-x)}{r},$$

$$(12)$$

and $f_A(r)$ is same as in Eq. (7). The results of our statistical analysis by taking $\cos(\beta-\alpha) = 0$ and $m_H = m_{H^\pm} = 300\,\mathrm{GeV}$ for Type-I and Type-X, and $m_H = m_{H^\pm} = 580\,\mathrm{GeV}$ for Type-II and Type-Y, are shown in Figures 5, 6, 7, and 8 and Table 2.

Not surprisingly, the Type-I model does not reproduce the data because it is similar to the SM. Type-Y is similar to Type-I except that the bottom quark contribution is enhanced. However, because of the lightness of the bottom quark, its contribution is not enough for the Type-Y model to explain the data. For Type-X, the large value of $\tan\beta$ enhances the tau-lepton contribution to the two-loop BZ diagram. The contribution from the bottom-quark in the BZ diagram provides a further enhancement in the Type-II model. Note that the Type-II parameters needed are excluded by constraints from $B_s \to \mu^+\mu^-$ and searches for $Z \to b\bar{b}A(b\bar{b})$ [15].

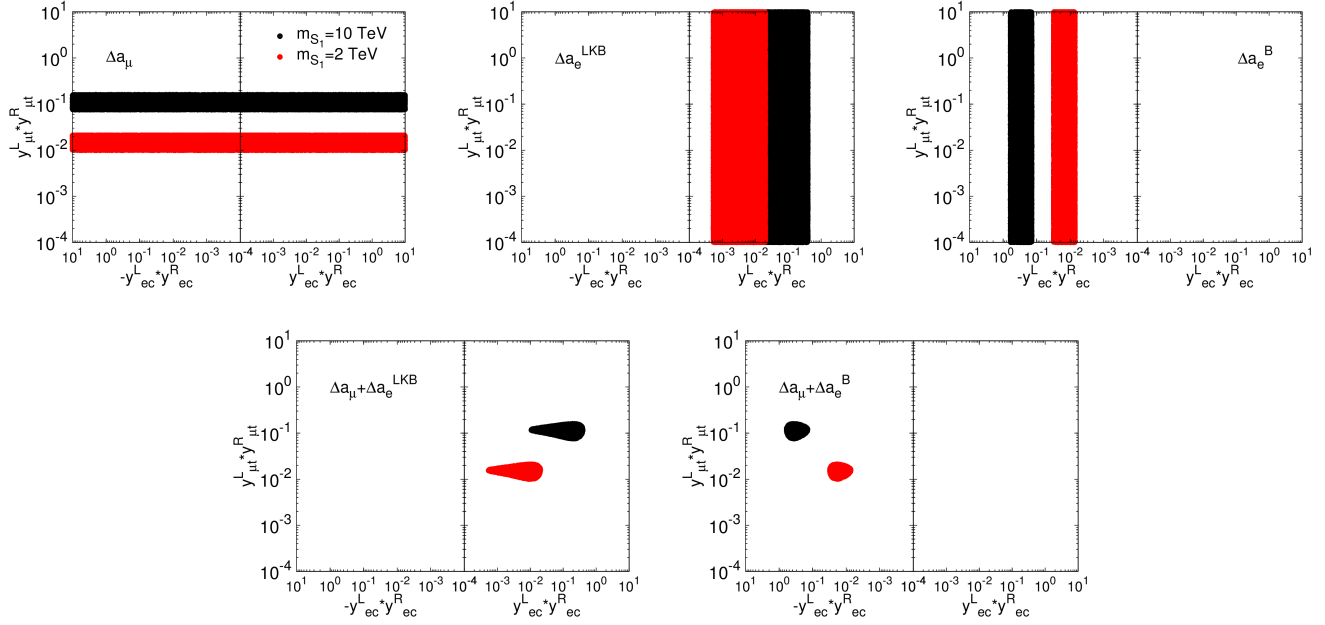**FIGURE 9:** S_1-**LQ:** The 1σ regions preferred by Δa_μ, Δa_e^{LKB}, and Δa_e^{B} (upper panels), and from a combined fit to Δa_μ and Δa_e^{LKB}, and Δa_μ and Δa_e^{B} (lower panels), for $m_{S_1} = 10$ TeV (black) $m_{S_1} = 2$ TeV (red).

4. LEPTOQUARKS

We consider a scalar leptoquark $S_1 \sim (\mathbf{3}, \mathbf{1}, -1/3)$ and a doublet leptoquark $(R_2)^T = (R_2^{5/3}, R_2^{2/3}) \sim (\mathbf{3}, \mathbf{2}, 7/6)$. Their couplings to quarks and leptons are specified in the "up-type" mass-diagonal basis because the "down-type" basis would violate constraints from $\mu \to e\gamma$ [21]. Then, the CKM matrix appears in the couplings with down-type quarks, and the interaction Lagrangian is [22]

$$
\begin{aligned}
\mathcal{L}^{S_1} \supset{} & y_{ij}^{SLQ} \left[\bar{e}_{L,i}^c u_{L,j} - V_{jk}^{\text{CKM}} \bar{\nu}_{L,i}^c d_{L,k} \right] S_1^\dagger \\
& + y_{ij}^{Seu} \bar{e}_{R,i}^c u_{R,j} S_1^\dagger + h.c., \\
\mathcal{L}^{R_2} \supset{} & y_{ij}^{RLu} \left[\bar{\nu}_{L,i} u_{R,j} R_2^{2/3,\dagger} - \bar{e}_{L,i} u_{R,j} R_2^{5/3,\dagger} \right] \\
& + y^{ReQ} \bar{e}_{R,i} \left[u_{L,j} R_2^{5/3,\dagger} + V_{jk}^{\text{CKM}} d_{L,k} R_2^{2/3,\dagger} \right] + h.c.
\end{aligned}
\tag{13}
$$

S_1 and $R_2^{5/3}$ have left- and right-handed couplings to the charge leptons and up-type quarks, and give a large contribution to a_ℓ under the condition $m_q \gg m_\ell$. We neglect the contribution of $R_2^{2/3}$, which only has left-handed couplings to down quarks. In the limit, $m_q \ll m_{\text{LQ}}$,

$$
\begin{aligned}
a_{\ell, S_1} &\simeq -\frac{m_\ell m_q}{4\pi^2 m_{S_1}^2} \left[\frac{7}{4} - 2\log\left(\frac{m_{S_1}}{m_q}\right) \right] \text{Re}(y_{\ell q}^{L*} y_{\ell q}^R), \\
a_{\ell, R_2} &\simeq \frac{m_\ell m_q}{4\pi^2 m_{R_2}^2} \left[\frac{1}{4} - 2\log\left(\frac{m_{R_2}}{m_q}\right) \right] \text{Re}(y_{\ell q}^{L*} y_{\ell q}^R),
\end{aligned}
\tag{14}
$$

where for S_1, $y_{ij}^R \equiv y_{ij}^{Seu}$ and $y_{ij}^L \equiv y_{ij}^{SLQ}$; and for $R_2^{5/3}$, $y_{ij}^R \equiv -y_{ij}^{RLu}$ and $y_{ij}^L \equiv y_{ij}^{ReQ}$. Note that a_ℓ requires both non-vanishing left- and right-handed Yukawa couplings. There is freedom to choose the texture of the Yukawa couplings $y_{ij}^{L,R}$. According to Eq. (14), heavier fermions contribute more to a_ℓ,

so we ignore the u quark and τ lepton. The remaining couplings are $y_{ec, et, \mu c, \mu t}^{L,R}$. However, if both y_{et} and $y_{\mu t}$ are non-zero, the m_t enhancement of $\mu \to e\gamma$ becomes incompatible with observation [22]. A non-zero $y_{\mu c}$ allows the LQ to couple to neutrinos and the s quark, thereby inducing $K^+ \to \pi^+ \nu\nu$ through CKM mixing. To obey these constraints we set $y_{et} = y_{\mu c} = 0$. Finally, we have the Yukawa couplings,

$$
y_{ij}^L \sim \begin{pmatrix} 0 & y_{ec}^L & 0 \\ 0 & 0 & y_{\mu t}^L \\ 0 & 0 & 0 \end{pmatrix}, \quad y_{ij}^R \sim \begin{pmatrix} 0 & y_{ec}^R & 0 \\ 0 & 0 & y_{\mu t}^R \\ 0 & 0 & 0 \end{pmatrix}.
\tag{15}
$$

Taking the couplings to be real, we scan the parameter space in two scenarios:

- S_1-**LQ:** We fix $m_{S_1} = 2, 10$ TeV, and vary $y_{ec}^L y_{ec}^R$ and $y_{\mu t}^L y_{\mu t}^R$. The results are shown in Figure 9 and Table 3.

- R_2-**LQ:** fixing $m_{R_2} = 2, 10$ TeV, and varying $y_{ec}^L y_{ec}^R$, and $y_{\mu t}^L y_{\mu t}^R$. The results are shown in Figure 10 and Table 3.

5. SUMMARY

In light of the recent measurement of the muon anomalous magnetic moment by the Muon $g - 2$ experiment, we examine three model frameworks as explanations of the $(g - 2)_{e,\mu}$ discrepancy with standard model expectations. We considered (i) axion-like particles with masses $\leq \mathcal{O}(1)\,\text{GeV}$ and couplings to charged leptons and photons, which yields a contribution to the 2-loop light-by-light diagram for $(g - 2)_{e,\mu}$. (ii) Two-Higgs-doublet models with four Yukawa structures: Type-I, II, X (lepton-specific), and Y (flipped), where the CP-odd scalar with mass $\leq \mathcal{O}(100)\,\text{GeV}$ gives the main contribution to $(g - 2)_{e,\mu}$ up to 2-loop Barr-Zee diagrams. (iii) Scalar leptoquarks, $S_1 \sim (\mathbf{3}, \mathbf{1}, -1/3)$ and $R_2 \sim (\mathbf{3}, \mathbf{2}, 7/6)$, where the
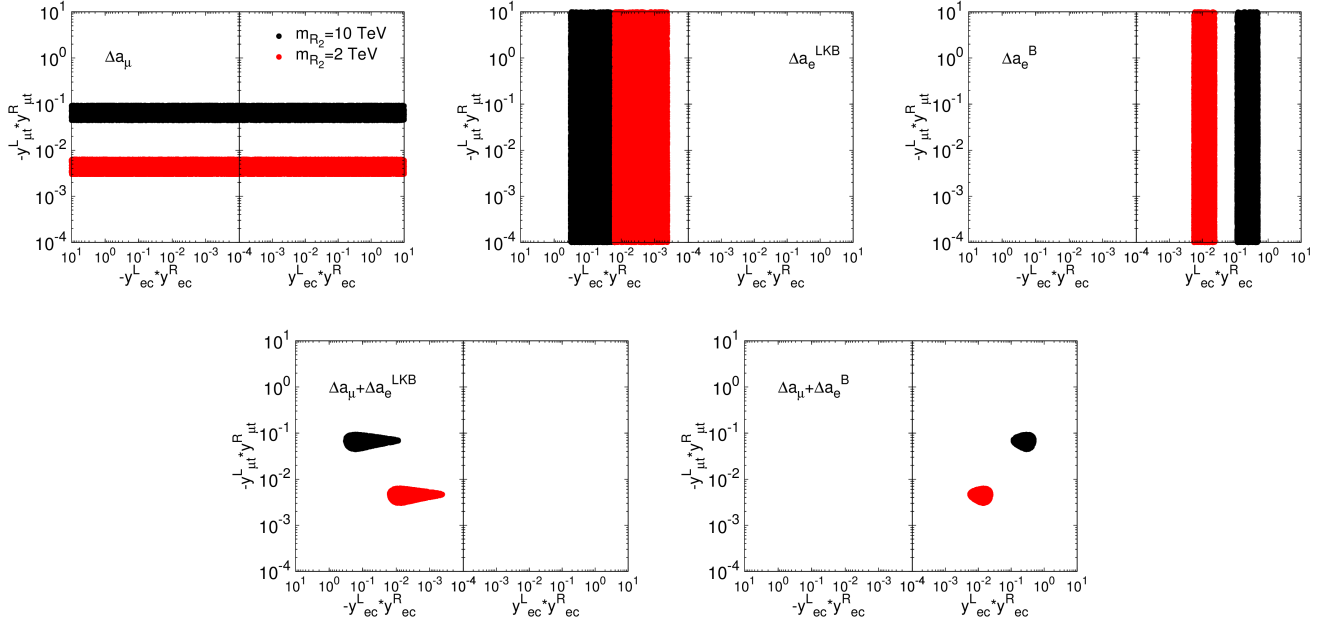
FIGURE 10: R_2**-LQ:** The 1σ regions preferred by Δa_μ, Δa_e^{LKB}, and Δa_e^{B} (upper panels), and from a combined fit to Δa_μ and Δa_e^{LKB}, and Δa_μ and Δa_e^{B} (lower panels), for $m_{R_2} = 10$ TeV (black) $m_{R_2} = 2$ TeV (red).

Yukawa couplings are assigned as up-type mass-diagonal basis to avoid constraints from $\mu \rightarrow e\gamma$. Then the mixed-chiral charm-electron and top-muon Yukawa couplings contribute to $(g-2)_e$ and $(g-2)_\mu$, respectively.

We find that accounting for other constraints, all scenarios except the Type-I, Type-II and Type-Y two-Higgs-doublet models easily accommodate the data.

ACKNOWLEDGMENTS

References

[1] G. W. Bennett *et al.* [Muon g-2 Collaboration], Phys. Rev. D **73**, 072003 (2006), [hep-ex/0602035].

[2] P. A. Zyla *et al.* [Particle Data Group], PTEP **2020**, no. 8, 083C01 (2020).

[3] T. Aoyama, N. Asmussen, M. Benayoun, J. Bijnens, T. Blum, M. Bruno, I. Caprini, C. M. Carloni Calame, M. Cè and G. Colangelo, *et al.* Phys. Rept. **887**, 1-166 (2020) [arXiv:2006.04822 [hep-ph]].

[4] S. Borsanyi, Z. Fodor, J. N. Guenther, C. Hoelbling, S. D. Katz, L. Lellouch, T. Lippert, K. Miura, L. Parato and K. K. Szabo, *et al.* [arXiv:2002.12347 [hep-lat]].

[5] B. Abi *et al.* [Muon g-2], Phys. Rev. Lett. **126**, 141801 (2021) [arXiv:2104.03281 [hep-ex]].

[6] L. Morel, Z. Yao, P. Cladé and S. Guellati-Khélifa, Nature **588**, no. 7836, 61 (2020).

[7] R. H. Parker, C. Yu, W. Zhong, B. Estey and H. Müller, Science **360**, 191 (2018), [arXiv:1812.04130 [physics.atom-ph]].

[8] T. Aoyama, M. Hayakawa, T. Kinoshita and M. Nio, Phys. Rev. Lett. **109**, 111807 (2012), [arXiv:1205.5368 [hep-ph]].

[9] T. Aoyama, T. Kinoshita and M. Nio, Atoms **7**, no. 1, 28 (2019).

[10] D. Hanneke, S. Fogwell and G. Gabrielse, Phys. Rev. Lett. **100**, 120801 (2008), [arXiv:0801.1134 [physics.atom-ph]].

[11] F. Jegerlehner and A. Nyffeler, Phys. Rept. **477**, 1 (2009), [arXiv:0902.3360 [hep-ph]].

[12] J. Prades, arXiv:0907.2938 [hep-ph].

[13] A. E. Dorokhov, A. E. Radzhabov and A. S. Zhevlakov, Eur. Phys. J. C **75**, no. 9, 417 (2015), [arXiv:1502.04487 [hep-ph]].

[14] J. D. Bjorken and S. Weinberg, Phys. Rev. Lett. **38**, 622 (1977); S. M. Barr and A. Zee, Phys. Rev. Lett. **65**, 21-24 (1990) [erratum: Phys. Rev. Lett. **65**, 2920 (1990)]

[15] E. J. Chun, EPJ Web Conf. **118**, 01006 (2016) [Pramana **87**, no. 3, 41 (2016)], [arXiv:1511.05225 [hep-ph]].

[16] W. J. Marciano, A. Masiero, P. Paradisi and M. Passera, Phys. Rev. D **94**, no. 11, 115033 (2016), [arXiv:1607.01022 [hep-ph]].

[17] J. Jaeckel and M. Spannowsky, Phys. Lett. B **753**, 482 (2016), [arXiv:1509.00476 [hep-ph]].

[18] K. Mimasu and V. Sanz, JHEP **1506**, 173 (2015) [arXiv:1409.4792 [hep-ph]].

[19] G. C. Branco, P. M. Ferreira, L. Lavoura, M. N. Rebelo, M. Sher and J. P. Silva, Phys. Rept. **516**, 1 (2012), [arXiv:1106.0034 [hep-ph]].

[20] M. Misiak and M. Steinhauser, Eur. Phys. J. C **77**, no.3, 201 (2017) [arXiv:1702.04571 [hep-ph]].

[21] I. Doršner, S. Fajfer and S. Saad, Phys. Rev. D **102**, no. 7, 075007 (2020), [arXiv:2006.11624 [hep-ph]].

[22] I. Bigaran and R. R. Volkas, Phys. Rev. D **102**, no. 7, 075037 (2020), [arXiv:2002.12544 [hep-ph]].